Detection of Lumen-Intima Interface of Posterior Wall for Measurement of Elasticity of the Human Carotid Artery

Hideyuki Hasegawa, *Member, IEEE*, Hiroshi Kanai, *Member, IEEE*, and Yoshiro Koiwa

***Abstract*—In our series of studies on noninvasive assessment of the regional elasticity of the arterial wall, the displacement gradient (change in thickness) of the arterial wall caused by the heartbeat was measured by the phased-tracking method. Because the displacement gradient corresponds to the strain due to the change in blood pressure, the elasticity can be evaluated from the displacement gradient of the arterial wall and the blood pressure, which are noninvasively measured at the upper arm. In the measurement of the elasticity of the arterial wall by our method, the region in which the elastic modulus is estimated must be assigned beforehand; currently, the lumen-intima boundary of the arterial wall is manually determined by the operator. For the real-time measurement of the elasticity of the arterial wall, a fast, automated method is necessary for detection of the boundary. In this paper, a cost function is proposed for differentiation of the arterial wall from the lumen. The proposed cost function was applied to ultrasound data, which were noninvasively obtained for five human carotid arteries. In comparison with the case of detection using only the amplitude of the echo, the root mean square error between the automatically detected lumen-intima boundary and the manually assigned boundary was significantly improved by using the proposed cost function. Furthermore, the lumen-intima boundary was automatically detected in a short period. Such a method is required for real-time measurement of the elasticity of the arterial wall, though detection of the outer boundary of the adventitia, which is not described in this paper, is also necessary to realize real-time elasticity measurement by our method.**

I. Introduction

The steady increase in the number of patients with myocardial infarction or cerebral infarction, both of which are considered to be mainly caused by atherosclerosis, is becoming a serious problem [1], [2]. Therefore, it is important to diagnose atherosclerosis in the early stage. Computed tomography (CT), magnetic resonance imaging (MRI), and ultrasonic diagnostic equipment are used for the diagnosis of atherosclerosis [3]–[5]. However, they provide information only on the shape of the artery, such as the diameter of the lumen. In addition, CT and MRI are not suitable for repetitive diagnosis due to the exposure to radiation and the high expense. However, the diameter of the lumen, which can be measured by these methods, is not changed by early-stage atherosclerosis [6].

Manuscript received September 19, 2002; accepted July 31, 2003.

H. Hasegawa and H. Kanai are with the Graduate School of Engineering, Tohoku University, Sendai 980-8579, Japan (e-mail: hasegawa@us.ecei.tohoku.ac.jp).

Y. Koiwa is with the Graduate School of Medicine, Tohoku University, Sendai 980-8575, Japan.

Because there are significant differences between the elastic moduli of the normal arterial walls and those affected by atherosclerosis [7], [8], evaluation of the elasticity of the arterial wall is useful for diagnosis of early-stage atherosclerosis [9]. In addition to diagnosis of early-stage atherosclerosis, it also is important to diagnose vulnerability of atherosclerotic plaque because the rupture of such plaque causes acute myocardial infarction and cerebral infarction [10]–[12]. Evaluation of mechanical properties, such as elasticity of atherosclerotic plaque, is useful for the diagnosis of vulnerability of such plaque. Using standard ultrasonic diagnostic equipment, intima-media thickness (IMT) can be evaluated noninvasively [5]. However, the mechanical properties of atherosclerotic plaque cannot be determined.

To measure the elasticity of the arterial wall, the pulse wave velocity (PWV) method has been developed as a technique for the noninvasive diagnosis of atherosclerosis [13]. In this method, the elasticity of the arterial wall is evaluated by measuring the velocity of the pressure wave propagating from the heart to the femoral artery. Though it is useful in terms of noninvasive evaluation of the elasticity, regional elasticity cannot be evaluated due to a low spatial resolution of tens of centimeters, which almost corresponds to the distance from the heart to the femoral artery.

To improve the spatial resolution in measurement of PWV, we previously proposed a method to accurately measure the propagation velocity of vibrations on the arterial wall using ultrasound [14]–[16]. Using this method, the PWV between two adjacent points, which are separated from each other by several centimeters, can be noninvasively measured by estimating the time delay between the resultant vibrations at these two points set along the axial direction of the artery.

Methods for measurement of the change in artery diameter have been proposed [17]–[21] in order to obtain the circumferential distensibility of the arterial wall in the plane that is perpendicular to the axial direction of the artery. By assuming the artery to be a cylindrical shell, the average elasticity of the entire circumference of the plane can be evaluated [22]–[24]. However, the regional elasticity of atherosclerotic plaque cannot be obtained by these methods because an artery with such plaque cannot be assumed to be a cylindrical shell with uniform wall thickness.

Recently, Bonnefous [25] measured the displacement and strain around carotid atherosclerotic plaque using tis-

sue Doppler imaging. He showed the inhomogeneity of the displacement upstream and downstream of atherosclerotic plaque and suggested that the arterial wall motion has potential for evaluation of plaque vulnerability.

De Korte *et al.* [26] and Céspedes *et al.* [27] evaluated the elasticity of coronary atherosclerotic plaque using intravascular ultrasonography (IVUS). They compared the measured elasticity distribution with the pathological image and showed that it was possible to characterize tissues in atherosclerotic plaque by measuring its elasticity.

In our series of studies, we have been attempting to evaluate the elasticity of a local region, even in the case of atherosclerotic plaque using transcutaneous ultrasound. Such a technique for measurement of the spatial distribution of the regional elasticity would be useful for diagnosis of the vulnerability of such plaque as well as for the diagnosis of early-stage atherosclerosis. In our method, the small displacement gradient (change in thickness) of the arterial wall due to the heartbeat was accurately measured in each local region that corresponds to the focal area of the ultrasonic beam [15], [28]–[30]. From the resultant displacement gradient, the regional strain and the elasticity of the arterial wall were noninvasively evaluated [31], [32].

In the measurement of the elasticity of the arterial wall by our method, the region in which the elastic modulus is estimated must be assigned; currently, the lumen-intima boundary of the arterial wall is manually determined by an operator. For the real-time measurement of the elasticity of the arterial wall, an automated method for detection of the boundary of the arterial wall in a short time is indispensable.

In the literature, several methods have been proposed for detection of the arterial wall boundary using the ultrasound B-mode image. For measurement of the flow-mediated dilation response [33], methods for detection of the boundary of the arterial wall have been proposed for measurement of the arterial diameter [34]–[37]. Fan *et al.* [34] used an adaptive template, which approximated the envelopes of echoes reflected by the lumen-intima interface and media-adventitia interface. Stadler *et al.* [35] estimated the arterial diameter from the B-mode image of the artery that was obtained by rotating the scan plane slightly off of the vessel axis. Under such conditions, the cross section of the artery can be modeled as an ellipse, and the arterial diameter is obtained by estimating the size of the ellipse. Beux *et al.* [36] used the gradient of the intensity in the B-mode image of the artery. Newey and Nassiri [37] estimated the arterial diameter from the B-mode image using the neural network. In these methods for measurement of the flow-mediated dilation response, the media-adventitia boundary was used for measurement of the arterial diameter, and the lumen-intima boundary was not used because the amplitude of the echo reflected by the media-adventitia interface is usually high and stable in comparison with that from the lumen-intima interface. However, the lumen-intima boundary must be determined for measurement of the arterial elasticity in our method.

For measurement of the IMT, several methods have been proposed for detection of the lumen-intima boundary using the ultrasound B-mode image [38], [39]. In these methods, the lumen-intima boundary is precisely detected using dynamic programming [38] and the active surface technique [39]. However, such sophisticated methods are time consuming and, therefore, not suitable for the real-time measurement of the elasticity of the arterial wall. Hoeks *et al.* [40] and Willekes *et al.* [41] proposed a method for detection of the IMT using the time averaged envelope of the echo. In this method, the envelope of the echo is averaged with compensation of the motion of the arterial wall using the wall tracking method [19]. However, displacement of each sampled point along the ultrasonic beam must be estimated before detection of the lumen-intima boundary in order to compensate for the motion of the arterial wall.

In this paper, a new method is proposed for detection of the lumen-intima boundary of the posterior wall of the human carotid artery during a sufficiently short period. Such a method is necessary for real-time measurement of the elasticity of the arterial wall. However, this method is not sufficient to realize the real-time elasticity measurement by our method because the luminal boundary of the anterior wall and the outer boundary of adventitia also are needed.

II. Methods

A. Off-Line and Manual Processing of Ultrasonic Data for Assessment of Arterial Wall Elasticity

In this section, an example of off-line and manual processing of ultrasonic data for assessment of arterial wall elasticity is shown to illustrate the need for automatic boundary detection.

For measurement of the elasticity of the arterial wall, the displacement of an object is estimated using the quadrature demodulated signal of the received ultrasonic wave. A quadrature demodulated signal is obtained using a 7.5 MHz linear-type ultrasonic probe of ultrasonic diagnostic equipment (Toshiba SSH-140A, Toshiba Corporation, Tokyo, Japan). Because ultrasonic beams are scanned at 60 positions along the axial direction of the artery, with spacing of 300 μm at a pulse repetition frequency of 12 kHz, the frame rate becomes 12 kHz/60 = 200 Hz. The in-phase and quadrature signals are simultaneously A/D converted with a 12-bit A/D converter at a sampling frequency of 10 MHz.

From the acquired demodulated signal, $z(t; d; \ell)$, reflected at a time, t, at a depth, d, at a beam position, ℓ, the elasticity of each local region in the arterial wall are obtained as follows.

1. Manual Assignment of Initial Depths of Lumen-Intima Boundary and Outer Boundary of Adventitia: The lumen-intima boundary and the outer boundary of adventitia must be assigned manually with respect to the pos-

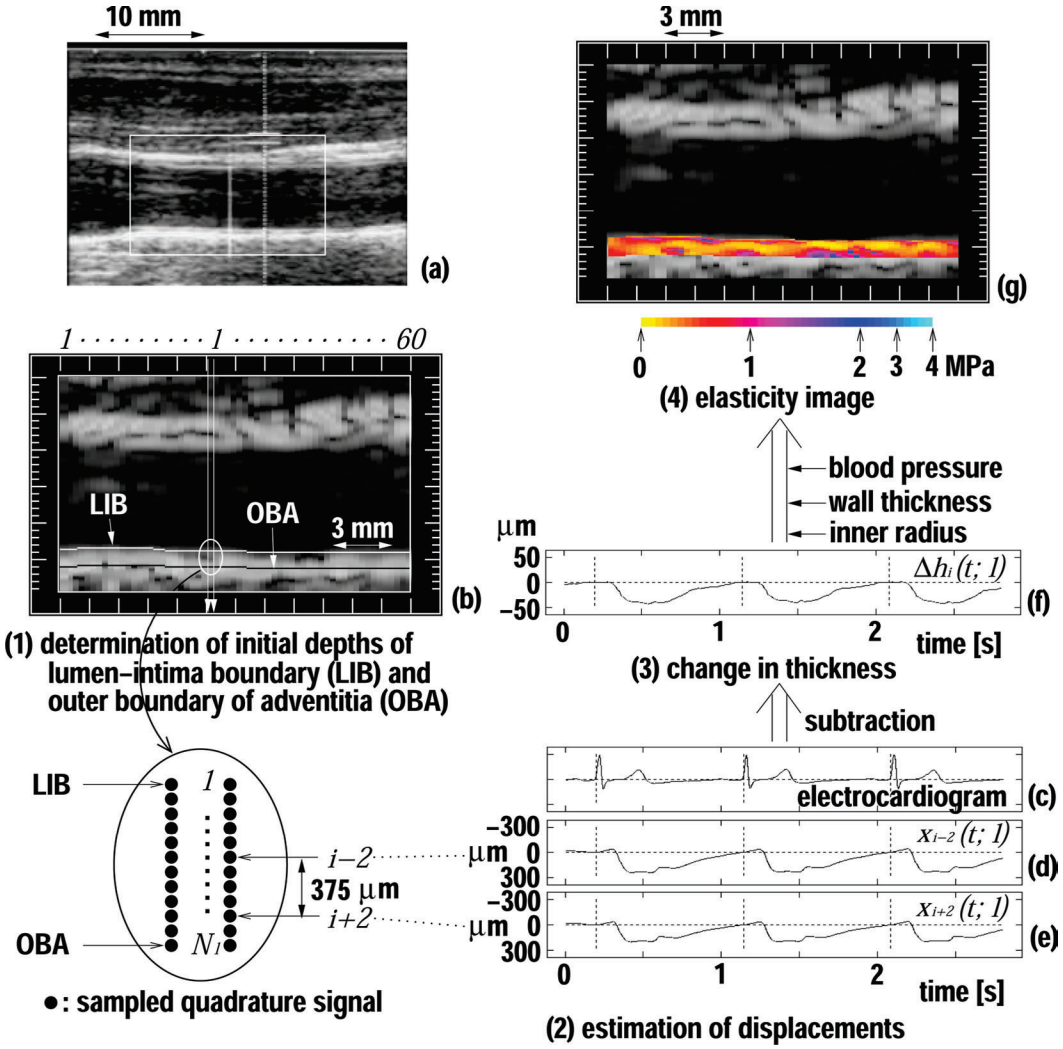

Fig. 1. Procedure for measuring the elasticity of the arterial wall. (a) B-mode image of carotid artery of a 29-year-old male obtained by standard ultrasonic diagnostic equipment. (b) Manually assigned the lumen-intima boundary (LIB) and the outer boundary of adventitia (OBA) superimposed on the B-mode image reconstructed from the quadrature demodulated signal. (c) Electrocardiogram. (d) Displacement, $x_{i-2}(t;\ell)$, of $(i-2)$-th point. (e) Displacement, $x_{i+2}(t;\ell)$, of $(i+2)$-th point. (f) Displacement gradient (Change in thickness), $\Delta h_i(t;\ell)$, of i-th layer. (g) Elasticity image.

terior wall to specify where the arterial wall is. This is done by manually tracing the B-mode image at time t_0 of the R-wave of the electrocardiogram reconstructed from the acquired quadrature demodulated signal as shown in Fig. 1(b). In Fig. 1, a data set, measured at the carotid artery of 29-year-old male, is shown as an example of elasticity measurement.

In some cases, the lumen-intima boundary of the anterior wall cannot be clearly recognized in the B-mode image due to the influence of the multiple reflection from the anterior wall and scattering from the tissue between the anterior wall and the skin surface. Therefore, we focus our attention on the posterior wall in the measurement of the arterial wall elasticity.

2. Estimation by the Phased Tracking Method of the Displacement Gradient (Change in Thickness) of the Arterial Wall Due to the Beating of the Heart: With respect to N_ℓ sampled points between the assigned lumen-intima boundary and the outer boundary of adventitia along the ℓ-th ultrasonic beam, the displacement of each point, $x_i(t;\ell)(i = 1, 2, \ldots, N_\ell)$, is estimated using the phased-tracking method [14]. For estimation of the displacement, the phase shift, $\Delta\psi_i(t;\ell)$, between two consecutive echoes is obtained from the complex cross-correlation function calculated for $M_c + 1$ samples in the depth direction as shown in (1) (see next page), where D and T_r are the interval of sampled points in the depth direction and the pulse repetition interval, respectively, and $*$ represents the complex conjugate. In (1), $M_c + 1$ is set at 5 ($= 0.4\ \mu$s) in consideration of the pulse length of 0.46 μs. In estimation of the phase shift by (1), the object position is tracked by integrating the average velocity, $v_i(t + T_r/2;\ell)$, during the pulse repetition interval, T_r, as follows:

$$\begin{aligned}\widehat{x}_i(t+T_r;\ell) &= \widehat{x}_i(t;\ell) + \widehat{v}_i\left(t+\frac{T_r}{2};\ell\right)\times T_r \\ &= \widehat{x}_i(t;\ell) + \frac{c_0}{2\omega_0}\Delta\widehat{\psi}_i(t), \quad (x_i(t_0;\ell)=0), \end{aligned} \tag{2}$$

$$e^{j\Delta\widehat{\psi}_i(t;\ell)} = \frac{\sum_{m=-M_c/2}^{M_c/2} z(t+T_r; d+x_i(t;\ell)+mD;\ell)\cdot z^*(t; d+x_i(t;\ell)+mD;\ell)}{\left|\sum_{m=-M_c/2}^{M_c/2} z(t+T_r; d+x_i(t;\ell)+mD;\ell)\cdot z^*(t; d+x_i(t;\ell)+mD;\ell)\right|}, \quad (1)$$

where ω_0 and c_0 are the center angular frequency of the ultrasonic pulse and the speed of sound, respectively.

From the estimated displacement, $x_i(t;\ell)$, shown in Figs. 1(d) and (e), the displacement gradient (change in thickness) of the arterial wall due to the heartbeat is obtained. Because the spatial resolution of the ultrasound used is determined by the pulse length of 0.46 μs (= 354 μm at a speed of sound of 1540 m/s), the displacement gradient (change in thickness), $\Delta h_i(t;\ell)$, of each layer with a constant thickness of $h_0 = 385$ μm shown in Fig. 1(f) is obtained as follows:

$$\Delta h_i(t;\ell) = x_{i-2}(t;\ell) - x_{i+2}(t;\ell), \quad (i = 3, 4, \ldots, N_\ell - 2). \quad (3)$$

3. Reconstruction of the Elasticity Image: From the ratio of the maximum decrease in thickness during one heartbeat, $\Delta h_{i,\max}(\ell) = \max_t |\Delta h_i(t;\ell)|$, to the initial thickness, h_0, of the i-th layer, the maximum strain of the i-th layer is obtained by $\Delta\varepsilon_{i,\max}(\ell) = \Delta h_{i,\max}(\ell)/h_0$. Because the deformation is sufficiently small and is in the linear regime, it shows incremental strain in the radial direction. By assuming that the arterial wall is incompressible and that the blood pressure is applied normal to each layer, the elastic modulus, $E_{\theta,i}(\ell)$, of the i-th layer along the ℓ-th beam is approximately given by [32]:

$$E_{\theta,i}(\ell) = \frac{1}{2}\left(\frac{\rho_{i0}(\ell)}{h_0 \cdot N_\ell} + \frac{N_\ell - i + 1}{N_\ell}\right)\frac{\Delta p}{\Delta\varepsilon_{i,\max}(\ell)}, \quad (4)$$

where $\rho_{i0}(\ell)$ and Δp are the initial inner radius of curvature of the i-th layer along the ℓ-th beam at a time t_0 and the pulse pressure (difference between the systolic blood pressure and the diastolic blood pressure) measured at the upper arm, respectively. In (4), $E_{\theta,i}(\ell)$ represents the circumferential elastic modulus. Thus, a subscript θ indicates the circumferential direction of the artery. We assumed that the pressure in the arterial wall decreases linearly with the distance from the intimal side to the adventitia and that the arterial wall is almost isotropic. To determine $\rho_{i0}(\ell)$, the luminal boundary of the anterior wall also is assigned manually by tracing the B-mode image at a time t_0.

For the region with a length of 18 mm along the axis of the artery, the regional elasticity, $E_{\theta,i}(\ell)$, is estimated on the cross-sectional image. Because the reflected ultrasound is received at a sampling frequency of 10 MHz after quadrature demodulation, $E_{\theta,i}(\ell)$ is estimated at intervals of 77 μm in the depth direction by shifting the initial depth of each layer by one sampled point. By scanning the ultrasound beam, $E_{\theta,i}(\ell)$ is obtained at intervals of 300 μm in the axial direction of the artery, these intervals are determined by the spacing of the ultrasound beam. From the estimated $E_{\theta,i}(\ell)$ at intervals of 77 μm in the depth direction and 300 μm along the axis of the artery, the image of regional elasticity is obtained as shown in Fig. 1(g).

As described above, three boundaries—the lumen-intima boundaries of the posterior and anterior walls and the outer boundary of adventitia of the posterior wall—must be determined for measurement of the elasticity of the posterior wall by our method. In this paper, a method is proposed for automatic detection of the lumen-intima boundary of the posterior wall as a first step for automatic processing.

B. Cost Function for Differentiation of the Arterial Wall from the Lumen

1. Rationale for the Formulation of the Cost Function: In order to take motions of the arterial wall and blood particles, which cause the phase shift of the received ultrasonic wave, into account in this paper the lumen-intima boundary of the arterial wall is automatically determined using the quadrature demodulated signal, $z(t;d;\ell)$, which is obtained at a time, t, a depth, d, and an ultrasonic beam position, ℓ. Fig. 2(a) shows the B-mode image of the carotid artery of a 50-year-old male obtained by standard ultrasonic diagnostic equipment. The quadrature demodulated signal, $z(t;d;\ell)$, with respect to the preset region-of-interest (ROI) shown in Fig. 2(a) was acquired, and the B-mode image, which is reconstructed from the amplitude, $|z(t_0;d;\ell)|$, at time t_0 of the R-wave of the electrocardiogram, is shown in Fig. 2(b). In Fig. 2(b), there are 192 (in depth) $\times$ 60 (in lateral) = 11520 points within the ROI. In this paper, we search for the lumen-intima boundary of the posterior wall from the center to the end of the ROI by assuming that the center of the ROI corresponds to the lumen.

Fig. 3 shows the amplitude, $|z(t_0;d;\ell_1)|$, of the quadrature demodulated signal measured at beam position ℓ_1 as shown in Fig. 2(b). In Fig. 3, the amplitude, $|z(t_0;d;\ell)|$, of the quadrature demodulated signal is plotted as a function of depth, d. In position ℓ_1, the amplitude, $|z(t_0;d;\ell_1)|$, at the lumen is not small. This is thought to be due to multiple reflection from the anterior wall or scattering from the tissue between the skin surface and the anterior wall.

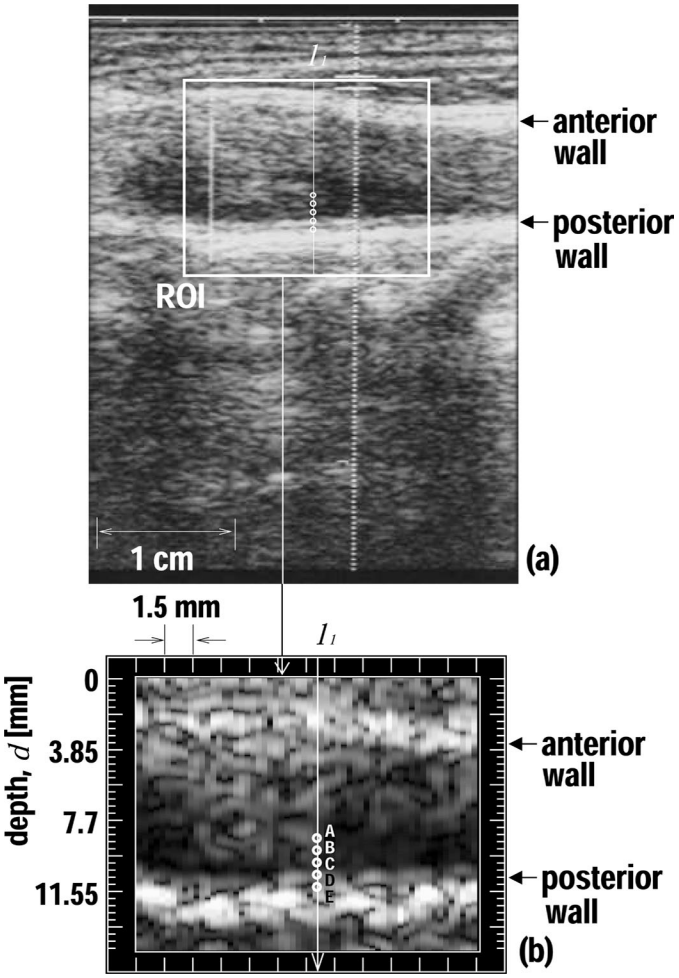

Fig. 2. (a) B-mode image of the human carotid artery of a 50-year-old male obtained by standard ultrasonic diagnostic equipment. (b) B-mode image within the ROI, which is reconstructed from the amplitude, $|z(t;d;\ell)|$, of the quadrature demodulated signal. Amplitude, $|z(t;d;\ell)|$, at position ℓ_1 is plotted as a function of depth in Fig. 3, and displacements of points A, B, C, D, and E are shown in Fig. 4(a).

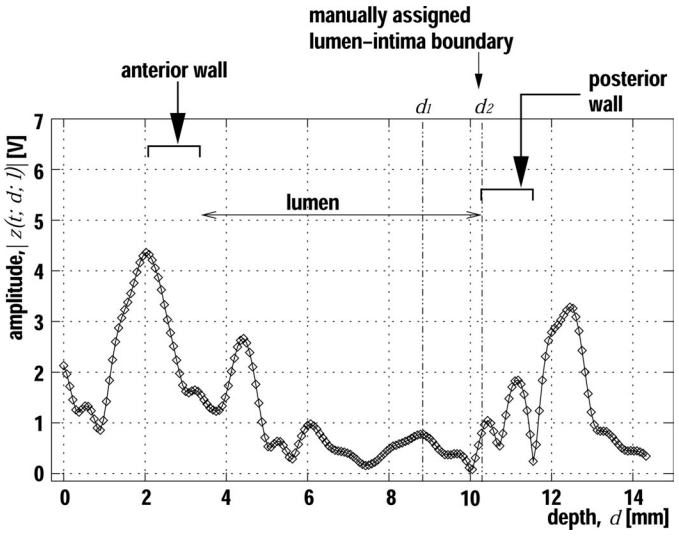

Fig. 3. Amplitude, $|z(t_0;d;\ell)|$, of the quadrature demodulated signal obtained at time t_0 of R-wave of the electrocardiogram at beam position ℓ_1 shown in Fig. 2(b).

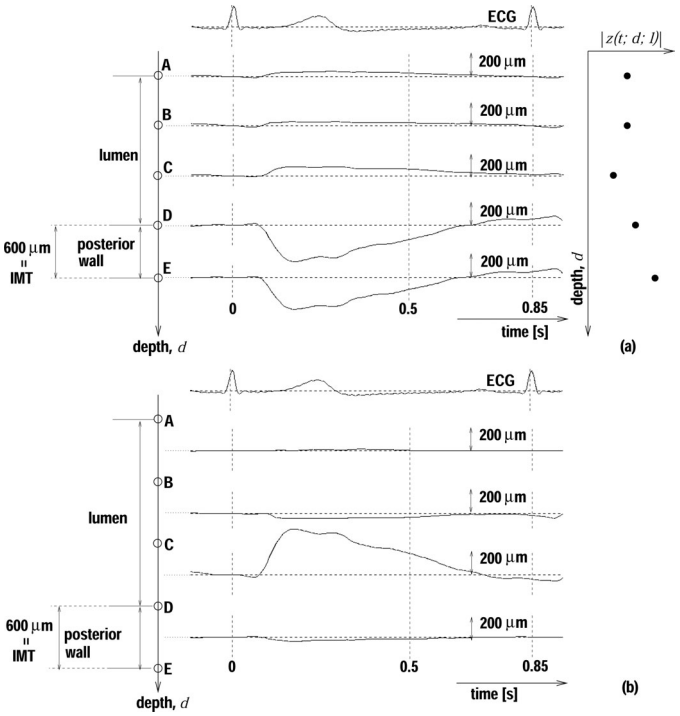

Fig. 4. (a) Displacement at each depth at beam position ℓ_1 measured by the phased-tracking method. (b) Displacement gradient at each depth at beam position ℓ_1.

In the case of position ℓ_1, when the lumen-intima boundary of the posterior wall is detected only from the amplitude, $|z(t_0;d;\ell_1)|$, of the quadrature demodulated signal, it is difficult to determine the optimal threshold level for the amplitude because the echo at the lumen-intima interface (at depth d_2, which is the manually assigned lumen-intima boundary) cannot be discriminated from the echo in the lumen (at depth d_1) only from the amplitude ($|z(t_0;d_2;\ell_1)|/|z(t_0;d_1;\ell_1)| = 1.0$). Therefore, it is difficult to detect the lumen-intima boundary only from the amplitude, $|z(t;d;\ell)|$, of the echo.

Fig. 4(a) shows the displacement at each depth along beam position ℓ_1 measured by the phased-tracking method for the same subject as shown in Fig. 2. The displacement at each depth is estimated by the phased-tracking method [14] described in Section II-A. In Fig. 4(a), the amplitude, $|z(t_0;d;\ell)|$, at the timing of the R-wave on the electrocardiogram is plotted in the right-hand side of Fig. 4(a). Points D and E in Fig. 4(a) correspond to the lumen-intima boundary and media-adventitia boundary of the posterior wall, respectively. The IMT was measured as being 0.6 mm from the B-mode image. Displacements were obtained at each depth with an interval of 600 μm, which is equivalent to the IMT. The arterial wall has displacement due to the change in blood pressure caused by the heartbeat. The displacement in the lumen at position ℓ_1 shows motion toward the skin surface at the time when the inner pressure increases. Such estimated motion is considered to be caused by the influence of the multiple reflection from the anterior wall or by scattering from the tissue between

the skin surface and the anterior wall, because they move toward the skin surface due to expansion of the artery.

Fig. 4(b) shows the displacement gradient at each depth obtained by subtracting displacements at the two neighboring points shown in Fig. 4(b). Using the displacement gradient, the difference between the arterial wall and lumen becomes larger in comparison with the displacement. Thus, the displacement gradient has potential to be effective for differentiation of the arterial wall from the lumen.

2. Formulation of the Cost Function: In this paper, we propose using the cost function, which reflects the difference in the displacement gradient as well as the difference in the amplitude of the reflected ultrasonic wave, for differentiation of the arterial wall from the lumen as follows. A complex signal, $\beta(t;d;d_{12};\ell)$, which represents the phase difference between two points at depths d and $d+d_{12}$ along an ultrasonic beam, ℓ, is defined by:

$$\beta(t;d;d_{12};\ell) = z^*(t;d;\ell)\cdot z(t;d+d_{12};\ell), \tag{5}$$

where $*$ denotes the complex conjugate. Due to the motion of the arterial wall and the blood flow in the lumen, $\beta(t;d;d_{12};\ell)$ at a time, t_0, of the R-wave is different from that after a time interval, T. Thus, the following is used as a model to estimate $\beta(t_0+T;d;d_{12};\ell)$ using $\beta(t_0;d;d_{12};\ell)$:

$$\widehat{\beta}(t_0+T;d;d_{12};\ell) = \beta(t_0;d;d_{12};\ell)\cdot\gamma(d;\ell), \tag{6}$$

where $\gamma(d;\ell)$ is a complex parameter of the model that corresponds to the changes in the amplitude and phase of $\beta(t;d;d_{12};\ell)$ from $\beta(t_0;d;d_{12};\ell)$ to $\beta(t_0+T;d;d_{12};\ell)$, and the phase, $\angle\gamma(d;\ell)$, of $\gamma(d;\ell)$ corresponds to the change in distance from d_{12}.

Let us define the mean squared difference, $\alpha(\gamma;d;\ell)$, between $\beta(t_0+T;d;d_{12};\ell)$ and its estimate, $\widehat{\beta}(t_0+T;d;d_{12};\ell)$, as follows:

$$\alpha(\gamma;d;\ell) = \frac{1}{(M+1)(N+1)}\sum_{m=-M/2}^{M/2}\sum_{n=-N/2}^{N/2} \Big|\beta(t_0+T;d+mD;d_{12};\ell+nL) - \beta(t_0;d+mD;d_{12};\ell+nL)\cdot\gamma(d;\ell)\Big|^2, \tag{7}$$

where D is the spacing (= 77 μm at a sound speed of 1540 m/s) between the succeeding sampled points in the depth direction. By considering the lateral continuity of the inner surface of the arterial wall in (7), $\alpha(\gamma;d;\ell)$ is averaged within $N+1$ ultrasonic beams, which are scanned with a spacing of L (= 300 μm). By increasing the number of ultrasonic beams to be averaged, the lateral continuity of the estimated lumen-intima boundary improves. However, a nonsmooth boundary, such as atherosclerotic plaque, cannot be detected when $\alpha(\gamma;d;\ell)$ is averaged by a large number of ultrasonic beams. Therefore, in this paper, minimum lateral averaging ($N=2$) is used.

The $\alpha(\gamma;d;\ell)$ shows the squared difference between $\beta(t_0+T;d;d_{12};\ell)$ and its estimate defined by (6). The $\beta(t;d;d_{12};\ell)$ changes dependent on the displacement and deformation of the object. Therefore, $\beta(t_0+T;d;d_{12};\ell)$ has components that cannot be estimated by the model defined by (6) when the object has displacement and deformation. If the object has no displacement and deformation, $\beta(t_0+T;d;d_{12};\ell)$ can be perfectly estimated from $\beta(t_0;d;d_{12};\ell)$, and $\alpha(\gamma;d;\ell)$ will be minimized to zero.

Eq. (7) can be rewritten as:

$$(M+1)(N+1)\cdot\alpha(\gamma;d;\ell) = A(d;\ell) + B(d;\ell)\cdot|\gamma(d;\ell)|^2 - C(d;\ell)\cdot\gamma^*(d;\ell) - C^*(d;\ell)\cdot\gamma(d;\ell), \tag{8}$$

where $A(d;\ell)$ and $B(d;\ell)$ are real constants defined by:

$$A(d;\ell) = \sum_{m=-M/2}^{M/2}\sum_{n=-N/2}^{N/2}|\beta(t_0+T;d+mD;d_{12};\ell+nL)|^2, \tag{9}$$

$$B(d;\ell) = \sum_{m=-M/2}^{M/2}\sum_{n=-N/2}^{N/2}|\beta(t_0;d+mD;d_{12};\ell+nL)|^2, \tag{10}$$

and $C(d;\ell)$ is a complex constant defined by:

$$C(d;\ell) = \sum_{m=-M/2}^{M/2}\sum_{n=-N/2}^{N/2}\beta^*(t_0;d+mD;d_{12};\ell+nL)\cdot\beta(t_0+T;d+mD;d_{12};\ell+nL). \tag{11}$$

By describing $C(d;\ell)$ and $\gamma(d;\ell)$ by the sum of their real and imaginary parts, C_r+jC_i and $\gamma_r+j\gamma_i$, respectively, the mean squared difference, $\alpha(\gamma;d;\ell)$, in (8) is described by:

$$(M+1)(N+1)\cdot\alpha(\gamma;d;\ell) = A(d;\ell) + B(d;\ell)\cdot\left(\gamma_r^2+\gamma_i^2\right) - 2\left(C_r\gamma_r + C_i\gamma_i\right). \tag{12}$$

By taking partial derivatives of $\alpha(\gamma;d;\ell)$ with respect to γ_r and γ_i:

$$\frac{1}{2}(M+1)(N+1)\cdot\frac{\partial\alpha}{\partial\gamma_r} = B\gamma_r - C_r, \tag{13}$$

$$\frac{1}{2}(M+1)(N+1)\cdot\frac{\partial\alpha}{\partial\gamma_i} = B\gamma_i - C_i. \tag{14}$$

In order to determine the complex variable $\widehat{\gamma}(d;\ell)$, which achieves the minimum of $\alpha(\gamma;d;\ell)$, by setting the right-hand sides of (13) and (14) to zero as shown in (15) (see next page).

By substituting $\widehat{\gamma}(d;\ell)$ of (15) into (8), the minimum value, $\alpha_{\min}(d;\ell)$, of $\alpha(\gamma;d;\ell)$ is given by (16) (see next page).

The value of $\alpha_{\min}(d;\ell)$ increases when the change in the amplitude, the displacement, and the displacement gradient are large. If there is no change in the signal, $\beta(t;d;d_{12};\ell)$, (i.e., there is no displacement and change in thickness, and the amplitude of $\beta(t;d;d_{12};\ell)$ is constant.), $\alpha_{\min}(d;\ell)$ becomes zero. In this paper, $\alpha_{\min}(d;\ell)$ is used as a cost function, $f_{\text{cost}}(d;\ell)$, for detection of the lumen-intima boundary:

$$f_{\text{cost}}(d;\ell) = \alpha_{\min}(d;\ell). \tag{17}$$

$$\begin{aligned}\widehat{\gamma}(d;\ell) &= \frac{C(d;\ell)}{B} \\ &= \frac{\displaystyle\sum_{m=-M/2}^{M/2}\sum_{n=-N/2}^{N/2}\beta^*(t_0;d+mD;d_{12};\ell+nL)\cdot\beta(t_0+T;d+mD;d_{12};\ell+nL)}{\displaystyle\sum_{m=-M/2}^{M/2}\sum_{n=-N/2}^{N/2}\left|\beta(t_0;d+mD;d_{12};\ell+nL)\right|^2}.\end{aligned} \tag{15}$$

$$\begin{aligned}&\alpha_{\min}(d;\ell) \\ &= \min_{\gamma}\alpha(\gamma;d;\ell) \\ &= \frac{1}{(M+1)(N+1)}\left\{A(d;\ell)-\frac{|C(d;\ell)|^2}{B(d;\ell)}\right\} \\ &= \frac{1}{(M+1)(N+1)}\sum_{m=-M/2}^{M/2}\sum_{n=-N/2}^{N/2}\left|\beta(t_0+T;d+mD;d_{12};\ell+nL)\right|^2 \\ &\quad - \frac{\left|\displaystyle\sum_{m=-M/2}^{M/2}\sum_{n=-N/2}^{N/2}\beta^*(t_0;d+mD;d_{12};\ell+nL)\cdot\beta(t_0+T;d+mD;d_{12};\ell+nL)\right|^2}{(M+1)(N+1)\cdot\displaystyle\sum_{m=-M/2}^{M/2}\sum_{n=-N/2}^{N/2}\left|\beta(t_0;d+mD;d_{12};\ell+nL)\right|^2}.\end{aligned} \tag{16}$$

The distance, d_{12}, between two points is set at 616 μm (at a sound speed of 1540 m/s), which is larger than the pulse length of 0.46 μs (= 354 μm at a sound speed of 1540 m/s), and the cost function, $f_{\text{cost}}(d;\ell)$, is averaged within the pulse length ($M = 4$) in order to suppress the random signal.

Because the squared difference, $\alpha_{\min}(d;\ell)$, is used as the cost function, $f_{\text{cost}}(d;\ell)$, the cost function depends on the change in $\beta(t;d;d_{12};\ell)$ between t_0 and t_0+T. Due to the finite pulse length of 354 μm, the change in $\beta(t;d;d_{12};\ell)$ becomes large when the displacement or the displacement gradient becomes comparable to the pulse length. Therefore, the cost function, $f_{\text{cost}}(d;\ell)$, becomes large at the lumen-intima boundary because the displacement and displacement gradient are comparable to the pulse length as shown in Fig. 4. However, in the lumen, $f_{\text{cost}}(d;\ell)$ becomes small because the displacement and displacement gradient are small. Thus, the proposed $f_{\text{cost}}(d;\ell)$ is useful for differentiation of the arterial wall from the lumen.

In (16), t_0 and T are set at the time of the R-wave and 500 ms, respectively, to take the difference between motions of the arterial wall and blood particles into account. After about 500 ms from the R-wave of the electrocardiogram [the time is shown by the vertical dashed line in Fig. 4(a)], the artery is expanded due to an increment in the blood pressure, and the blood particles, which are inside the ultrasonic beam at time t_0 of the R-wave, are expelled by the blood flow. Typically, systole lasts for about 300 ms, during which the displacement and the displacement gradient become maximum. Although larger displacement is desirable to increase the cost function, the position of the peak in the cost function around the posterior wall becomes more dependent on the wall displacement than that of the lumen-intima boundary at the time of the R-wave. Because the position of lumen-intima boundary at the time of the R-wave of the electrocardiogram must be determined for elasticity measurement as described in Section II-A, the maximum displacement during systole is too large to determine the lumen-intima boundary at the time of the R-wave. Therefore, in this paper, T is set so as to be longer than systole.

In Fig. 5(a), the cost function, $f_{\text{cost}}(d;\ell_1)$, which is obtained at the beam position ℓ_1 as shown in Fig. 2(b), is plotted by diamonds. By using $f_{\text{cost}}(d;\ell)$ the difference between the arterial wall and lumen becomes larger ($f_{\text{cost}}(d_2;\ell_1)/f_{\text{cost}}(d_1;\ell_1) = 2067$) in comparison with the amplitude, $|z(t;d;\ell)|$, of the quadrature demodulated signal ($|z(t_0;d_2;\ell_1)|/|z(t_0;d_1;\ell_1)| = 1.0$) as shown in Fig. 3. From this result, $f_{\text{cost}}(d;\ell)$ could be effective for differentiation of the arterial wall from the lumen.

C. Differentiation by Spatial Derivative of the Cost Function

To increase the difference between the arterial wall and the lumen, the spatial derivative, $\mathrm{d}f_{\text{cost}}(d;\ell)$, of the cost

function is used for detection of the lumen-intima boundary.

Fig. 5(b) shows an enlarged view of the cost function, $f_{\rm cost}(d;\ell_1)$, around the posterior wall at the beam position ℓ_1, as shown in Fig. 2. In the lumen, the cost function has a small peak, which corresponds to the multiple reflection from the anterior wall or the scattering from the tissue between the anterior wall and the skin surface. Such peaks must be suppressed in order to reduce difficulties in setting the threshold level, ρ_f.

To suppress small peaks in the lumen, the spatial derivative, $\mathrm{d}f_{\rm cost}(d;\ell)$, of the cost function is averaged as the slope of the linear line obtained by applying the least-squares method to the measured cost function, $f_{\rm cost}(d;\ell)$, as follows:

$$\mathrm{d}f_{\rm cost}(d;\ell)=\frac{COV(d;\ell)}{VAR(d;\ell)}, \tag{18}$$

where

$$COV(d;\ell)=\frac{1}{(M_d+1)(N+1)}\sum_{m=-M_d/2}^{M_d/2}\sum_{n=-N/2}^{N/2}(d+mD)\cdot f_{\rm cost}(d+mD;\ell+nL)-\bar{d}\cdot\bar{f}_{\rm cost}, \tag{19}$$

$$VAR(d;\ell)=\frac{1}{M_d+1}\sum_{m=-M_d/2}^{M_d/2}(d+mD)^2-\bar{d}^{\,2}, \tag{20}$$

$$\bar{f}_{\rm cost}=\frac{1}{(M_d+1)(N+1)}\sum_{m=-M_d/2}^{M_d/2}\sum_{n=-N/2}^{N/2}f_{\rm cost}(d+mD;\ell+nL), \tag{21}$$

$$\bar{d}=\frac{1}{M_d+1}\sum_{m=-M_d/2}^{M_d/2}(d+mD). \tag{22}$$

In this paper, the spatial derivative, $\mathrm{d}f_{\rm cost}(d;\ell)$, is obtained as an average value within the region of 3 mm ($M_d=40$) in the depth direction in consideration of the width of the peak in the cost function, $f_{\rm cost}(d;\ell)$, which is about 3 mm around the posterior wall as shown in Fig. 5(a). In addition, as in (7), $\mathrm{d}f_{\rm cost}(d;\ell)$ is averaged within $N+1$ ($N=2$) scan lines by considering the lateral continuity of the inner surface of the arterial wall. By averaging the spatial derivative, undesirable small peaks in the lumen, whose width is less than 3 mm, are suppressed, and it becomes possible to set a sufficiently low threshold level. As shown in Fig. 3, the amplitude of echo reflected by the lumen-intima interface is not so large in comparison with that reflected by the media-adventitia interface. Therefore, a low threshold level is necessary to detect the lumen-intima boundary. If the threshold level is not sufficiently low, the media-adventitia boundary cannot be detected.

Figs. 6(a) and (b) show the spatial derivative, $\mathrm{d}f_{\rm cost}(d;\ell)$, of the cost function shown in Fig. 5(a) and an enlarged view of Fig. 6(a) around the posterior wall, respectively. Using the averaged spatial derivative, $\mathrm{d}f_{\rm cost}(d;\ell)$, undesirable small peaks in the lumen are suppressed.

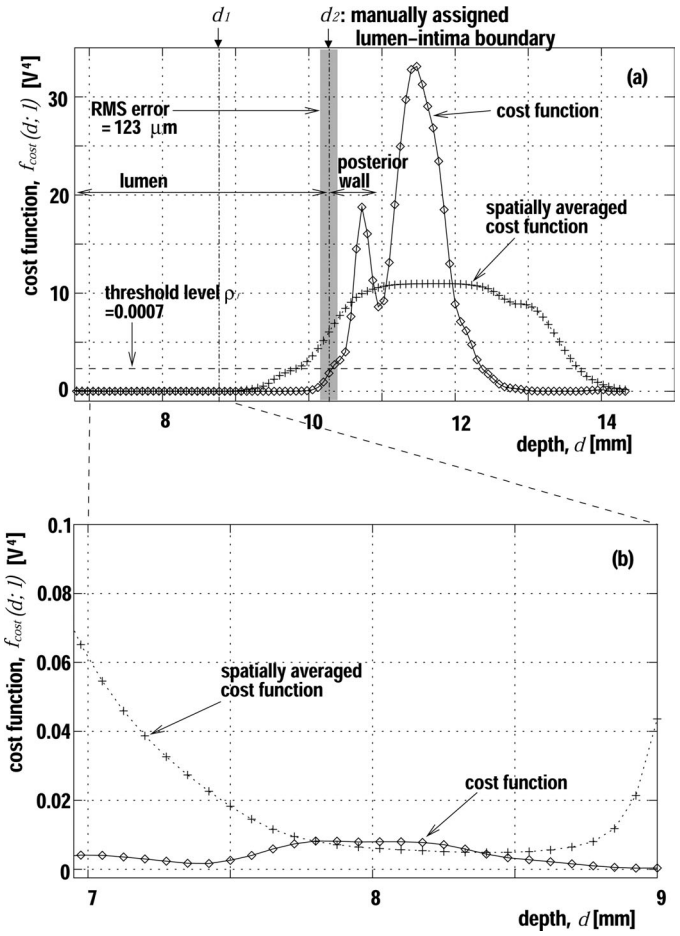

Fig. 5. (a) Cost function, $f_{\rm cost}(d;\ell_1)$, measured at beam position ℓ_1 is plotted as a function of depth. (b) Enlarged view of the cost function, $f_{\rm cost}(d;\ell)$, around the lumen-intima boundary at position ℓ_1.

Supposedly, small peaks in the lumen also can be suppressed by applying smoothing of the cost function. In Fig. 5, the cost function, which is spatially averaged within the area of the same size in calculation of spatial derivative by (18), also is plotted by crosses. Although the small peak in the lumen is suppressed, the smoothed cost function in the lumen also has a positive value, as does as that around the posterior wall. Therefore, the threshold level for the smoothed cost function becomes rather high in comparison with that for the spatial derivative. However, use of the high threshold level might result in detection of the media-adventitia boundary instead of the lumen-intima boundary. However, the spatial derivative, $\mathrm{d}f_{\rm cost}(d;\ell)$, has a negative value at the lumen as shown in Fig. 6. Therefore, the media-adventitia boundary is prevented from being detected by setting a positive threshold level, which can be set smaller than that for the smoothed cost function, for the spatial derivative.

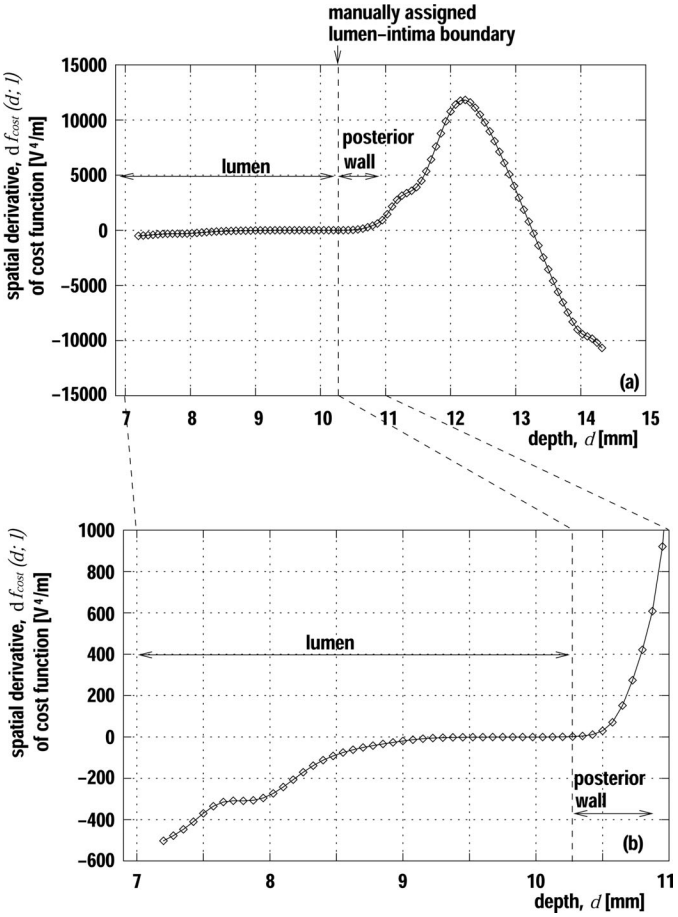

Fig. 6. (a) Spatial derivative, $\mathrm{d}f_{\mathrm{cost}}(d;\ell)$, of the cost function at beam position ℓ_1. (b) Enlarged view of (a).

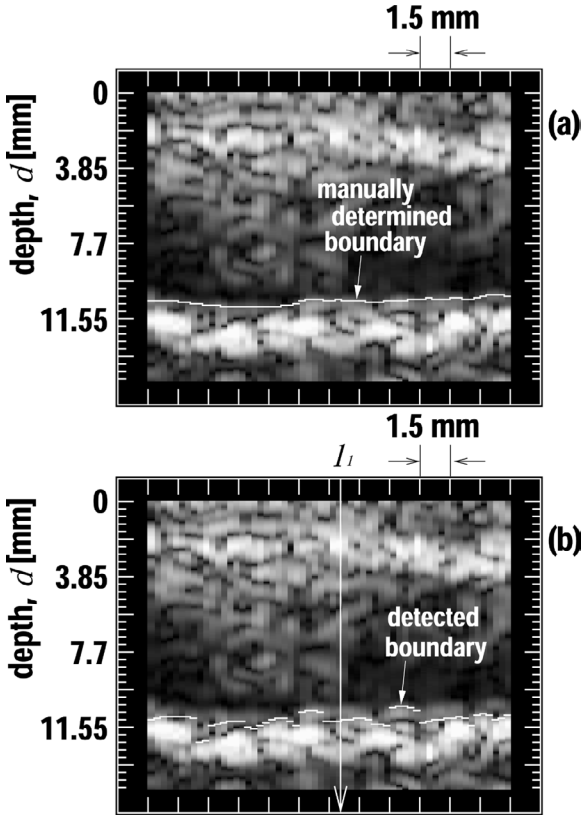

Fig. 7. (a) Manually determined lumen-intima boundary (50-year-old male). (b) Lumen-intima boundary detected by setting the threshold level to the amplitude, $|z(t;d;\ell)|$, of the quadrature demodulated signal.

III. In vivo Experimental Results for the Human Common Carotid Artery

A. Detection of Lumen-Intima Boundary by Setting the Threshold Level to the Amplitude of the Echo

In Fig. 7(b), the detected lumen-intima boundaries are shown as white lines, which are obtained by setting the threshold level to the amplitude, $|z(t;d;\ell)|$, of the quadrature demodulated signal. In the amplitude-based detection, $|z(t;d;\ell)|$ of the echo is spatially averaged within an area that is the same size as that used in calculation of the cost function in (16) and is normalized by the maximum amplitude within the ROI.

In Fig. 7(b), the threshold level, ρ_a, is determined by minimizing the root mean square (RMS) error, e_{RMS}, of the automatically detected lumen-intima boundary from the manually assigned boundary shown in Fig. 7(a). The RMS error, e_{RMS}, is defined by depths, $d_{\mathrm{cal}}(\ell)$ and $d_{\mathrm{man}}(\ell)$, of the automatically detected boundary and the manually assigned boundary at the ultrasonic beam position, ℓ, as follows:

$$e_{\mathrm{RMS}} = \sqrt{\frac{1}{N_b}\sum_{\ell=1}^{N_b} |d_{\mathrm{cal}}(\ell) - d_{\mathrm{man}}(\ell)|^2}, \qquad (23)$$

where N_b is the number of ultrasonic beam positions.

In Fig. 8, e_{RMS} of the automatically detected lumen-intima boundary is plotted as a function of the threshold level, ρ_a, and the optimum threshold level is determined to be 0.19. The threshold level, ρ_a, for the amplitude, $|z(t;d;\ell)|$, of the quadrature demodulated signal is expressed as a ratio of the threshold level to the maximum amplitude within the ROI. In Fig. 7(b), even under the optimum threshold setting, error of the detected boundary is still large ($e_{\mathrm{RMS}} = 555\ \mu$m). This result indicates that there are difficulties in setting the optimum threshold level to $|z(t;d;\ell)|$ of the echo because $|z(t;d;\ell)|$ at the lumen and that at the lumen-intima boundary are not sufficiently different. Thus, it is difficult to detect the lumen-intima boundary only from the amplitude of the echo.

B. Boundary Detection Using the Cost Function

In Fig. 9, the detected lumen-intima boundary is shown as a white line, which is obtained by setting the threshold level, ρ_f, to the cost function, $f_{\mathrm{cost}}(d;\ell)$. The threshold level for the cost function is expressed as a ratio of the threshold level to the maximum value of the cost function within the ROI. In Fig. 9, ρ_f is determined by minimizing e_{RMS} of the automatically detected lumen-intima boundary from the manually assigned boundary shown in Fig. 7(a). The optimum threshold level, ρ_f, is

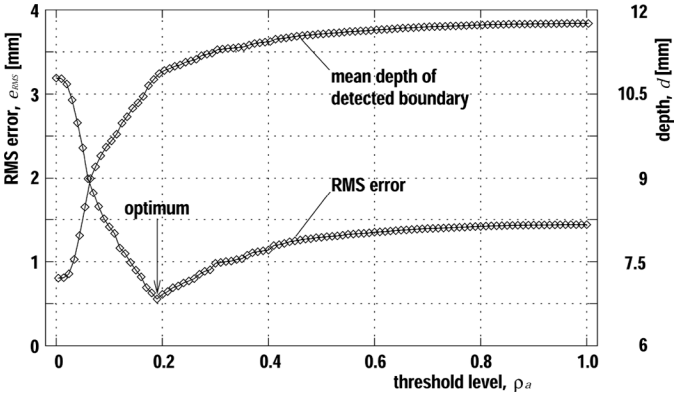

Fig. 8. RMS error, e_{RMS}, of detected lumen-intima boundary determined by setting the threshold level to the amplitude, $|z(t;d;\ell)|$, of the quadrature demodulated signal, is plotted as a function of the threshold level.

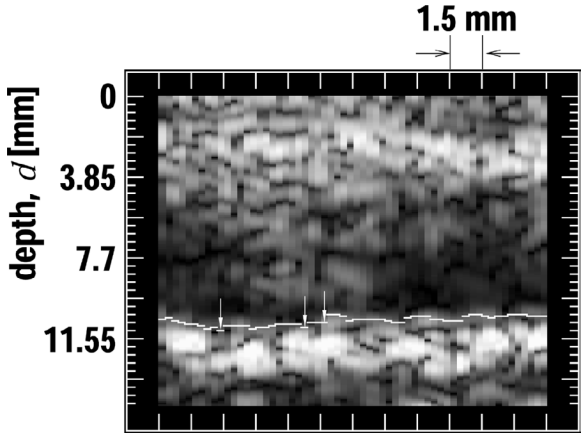

Fig. 9. Lumen-intima boundary detected by setting the threshold level to the cost function, $f_{\mathrm{cost}}(d;\ell)$ (same subject as shown in Fig. 7).

determined to be 0.0007 by minimizing e_{RMS} of the detected lumen-intima boundary. By using $f_{\mathrm{cost}}(d;\ell)$, e_{RMS} of the detected lumen-intima boundary is much improved ($e_{\mathrm{RMS}} = 123\ \mu$m). However, at some beam positions, large detection errors, which are indicated by white arrows in Fig. 9, still remain. The threshold level, ρ_f, must be lower than the value of $f_{\mathrm{cost}}(d;\ell)$ at the lumen-intima boundary to correctly detect the lumen-intima boundary at the beam position surrounded by the oval. However, a threshold level of 0.0007 is necessary to prevent the echo in the lumen from being detected. In order to reduce the threshold level, $f_{\mathrm{cost}}(d;\ell)$ in the lumen must be further suppressed.

C. Boundary Detection by Using the Spatial Derivative of the Cost Function

In Fig. 10, the lumen-intima boundary of the same subject as depicted in Fig. 9, which is detected using the spatial derivative, is shown as a white line. The RMS error, e_{RMS}, of the detected lumen-intima boundary is improved ($e_{\mathrm{RMS}} = 119\ \mu$m) by using the spatial derivative of the cost

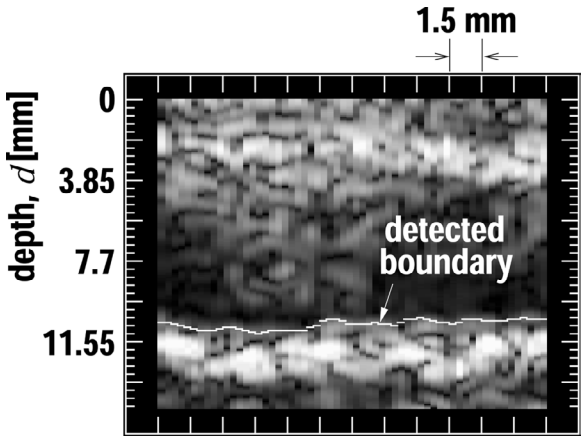

Fig. 10. Lumen-intima boundary of the posterior wall for the same data shown in Fig. 2 detected from the spatial derivative, $\mathrm{d}f_{\mathrm{cost}}(d;\ell)$, of the cost function.

function. The threshold level, ρ_{df}, is determined by minimizing e_{RMS} of the automatically detected lumen-intima boundary from the manually assigned boundary shown in Fig. 7(a). By minimizing e_{RMS} of the detected lumen-intima boundary, the optimum ρ_{df} is determined to be 0.00013, in which the threshold level is expressed as a ratio of the threshold level to the maximum value of the spatial derivative, $\mathrm{d}f_{\mathrm{cost}}(d;\ell)$, within the ROI.

D. Determination of the Threshold Level for Automatic Boundary Detection

To automatically detect the lumen-intima boundary, the threshold level must be determined beforehand. In this section, the threshold level is determined from the data sets obtained at carotid arteries of 21 subjects (male, 51±7 years old).

In Fig. 11, the threshold level, which gives minimum RMS error of the detected boundary from the manually determined boundary, is plotted for 21 data sets. Figs. 11(a), (b), and (c) show the threshold levels for the amplitude, $|z(t;d;\ell)|$, the cost function, $f_{\mathrm{cost}}(d;\ell)$, and the spatial derivative, $\mathrm{d}f_{\mathrm{cost}}(d;\ell)$, respectively. The mean values are used as threshold levels for automatic boundary detection in the following section.

In Fig. 11, RMS error of the detected boundary is improved using $f_{\mathrm{cost}}(d;\ell)$ or $\mathrm{d}f_{\mathrm{cost}}(d;\ell)$ in comparison with use of $|z(t;d;\ell)|$ of the echo. The standard deviation of the optimum threshold level for $\mathrm{d}f_{\mathrm{cost}}(d;\ell)$ shown in Fig. 11(c) is 35.3% to its mean value of 0.00015. This is smaller than 47.0% (mean: 0.0010) for $f_{\mathrm{cost}}(d;\ell)$. From these results, $\mathrm{d}f_{\mathrm{cost}}(d;\ell)$ is seen to have an advantage in fixing the threshold level.

E. Automatic Boundary Detection with a Constant Threshold Level

Using the threshold level determined in Section III-D, RMS errors of automatically detected boundary are evaluated with respect to four other subjects with and with-

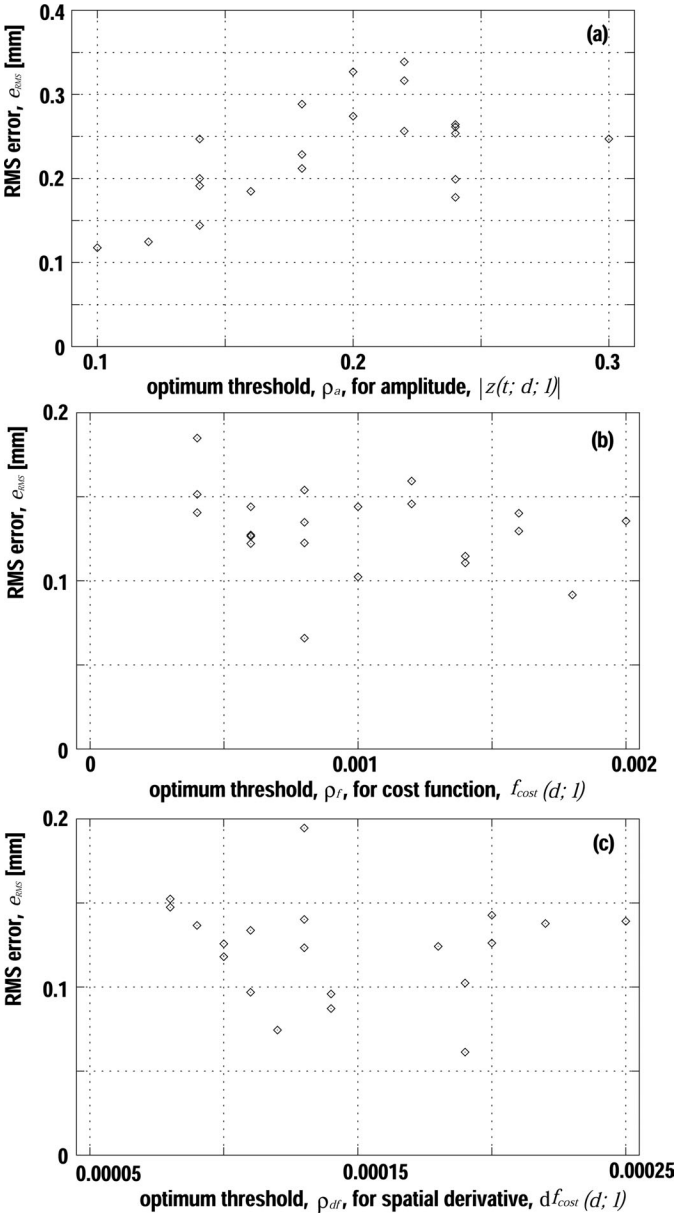

Fig. 11. RMS error, e_{RMS}, is plotted as a function of threshold level for 21 subjects. (a) Amplitude, $|z(t;d;\ell)|$, of echo. (b) Cost function, $f_{\mathrm{cost}}(d;\ell)$. (c) Spatial derivative, $\mathrm{d}f_{\mathrm{cost}}(d;\ell)$, of cost function.

out atherosclerotic plaque. In Fig. 12, the lumen-intima boundary for each subject, which was determined using $\mathrm{d}f_{\mathrm{cost}}(d;\ell)$, is shown as a white line. Good results were obtained for these four subjects as shown in Fig. 12, even when there was atherosclerotic plaque on the arterial wall [Fig. 12(b,4)].

The RMS errors, e_{RMS}, of the automatically detected lumen-intima boundaries of each subject—which are evaluated using the amplitude, $|z(t;d;\ell)|$, of the quadrature demodulated signal, cost function, $f_{\mathrm{cost}}(d;\ell)$, and spatial derivative, $\mathrm{d}f_{\mathrm{cost}}(d;\ell)$, of the cost function—are plotted in Fig. 13. For each subject, e_{RMS} is large when $|z(t;d;\ell)|$ of the quadrature demodulated signal is used. The RMS error, e_{RMS}, is reduced to about 0.1 mm using $\mathrm{d}f_{\mathrm{cost}}(d;\ell)$. It almost corresponds to the minimum resolution in distance measurement using standard ultrasonic diagnostic equipment. Therefore, the proposed method is sufficiently precise for detection of the lumen-intima boundary.

IV. Discussion

A. Elapsed Time for Calculating the Cost Function

When the ROI is composed of N_b beam positions and N_d sampled points in the direction of depth, the elapsed time, T_{total}, required for calculation of the spatial derivative, $f_{\mathrm{cost}}(d;\ell)$, of the cost function is estimated as follows:

$$T_{\mathrm{total}} = T_{\mathrm{cost}} + T_{\mathrm{spd}}, \tag{24}$$

where T_{cost} and T_{spd} are the elapsed time for calculation of the cost function, $f_{\mathrm{cost}}(d;\ell)$, and that for calculation of the spatial derivative, $f_{\mathrm{cost}}(d;\ell)$, respectively. In order to search for the lumen-intima boundary in the area from the center to the end of the ROI, $(N_d - M_d)/2$ spatial derivatives, $\mathrm{d}f_{\mathrm{cost}}(d;\ell)$, each of which is estimated from $M_d + 1$ cost functions, $f_{\mathrm{cost}}(d;\ell)$, by (18), must be obtained, and for this purpose, $(N_d + M_d)/2$ cost functions, $f_{\mathrm{cost}}(d;\ell)$, are calculated. Therefore, T_{cost} and T_{spd} are estimated as follows:

$$T_{\mathrm{cost}} = N_b \times \frac{N_d + M_d}{2} \times 21.7\ (\mu\mathrm{s}), \tag{25}$$

$$T_{\mathrm{spd}} = N_b \times \frac{N_d - M_d}{2} \times 24.3\ (\mu\mathrm{s}). \tag{26}$$

Using a typical data set, elapsed times of 21.7 μs and 24.3 μs in (25) and (26) are determined by measuring T_{cost} and T_{spd} using a computer with the Intel Pentium III 1.2 GHz CPU (Intel Corporation, Santa Clara, CA) and dividing measured T_{cost} and T_{spd} by $N_b(N_d + M_d)/2$ and $N_b(N_d - M_d)/2$ (number of data points), respectively. As a typical case, the data shown in Fig. 2(b) consist of 60 scan lines and 192 sampled points in the depth direction. In this case, the total elapsed time, T_{total}, is given by:

$$T_{\mathrm{total}} = 60 \times \frac{192 + 40}{2} \times 21.7 \times 10^{-3} + 60 \times \frac{192 - 40}{2} \times 24.3 \times 10^{-3} = 262\ \mathrm{ms}. \tag{27}$$

The typical elapsed time of 0.26 s for the calculation is applicable for real-time measurement of the elasticity of the arterial wall.

B. Evaluation of Repeatability

To evaluate the repeatability of the proposed method, in vivo experiments at the carotid artery were conducted for three subjects (29-year-old male, 23-year-old male, and 21-year-old male). Measurements were performed five times for each subject, and the RMS error of the boundary automatically detected from the manually assigned boundary was evaluated for each measurement. The threshold level,

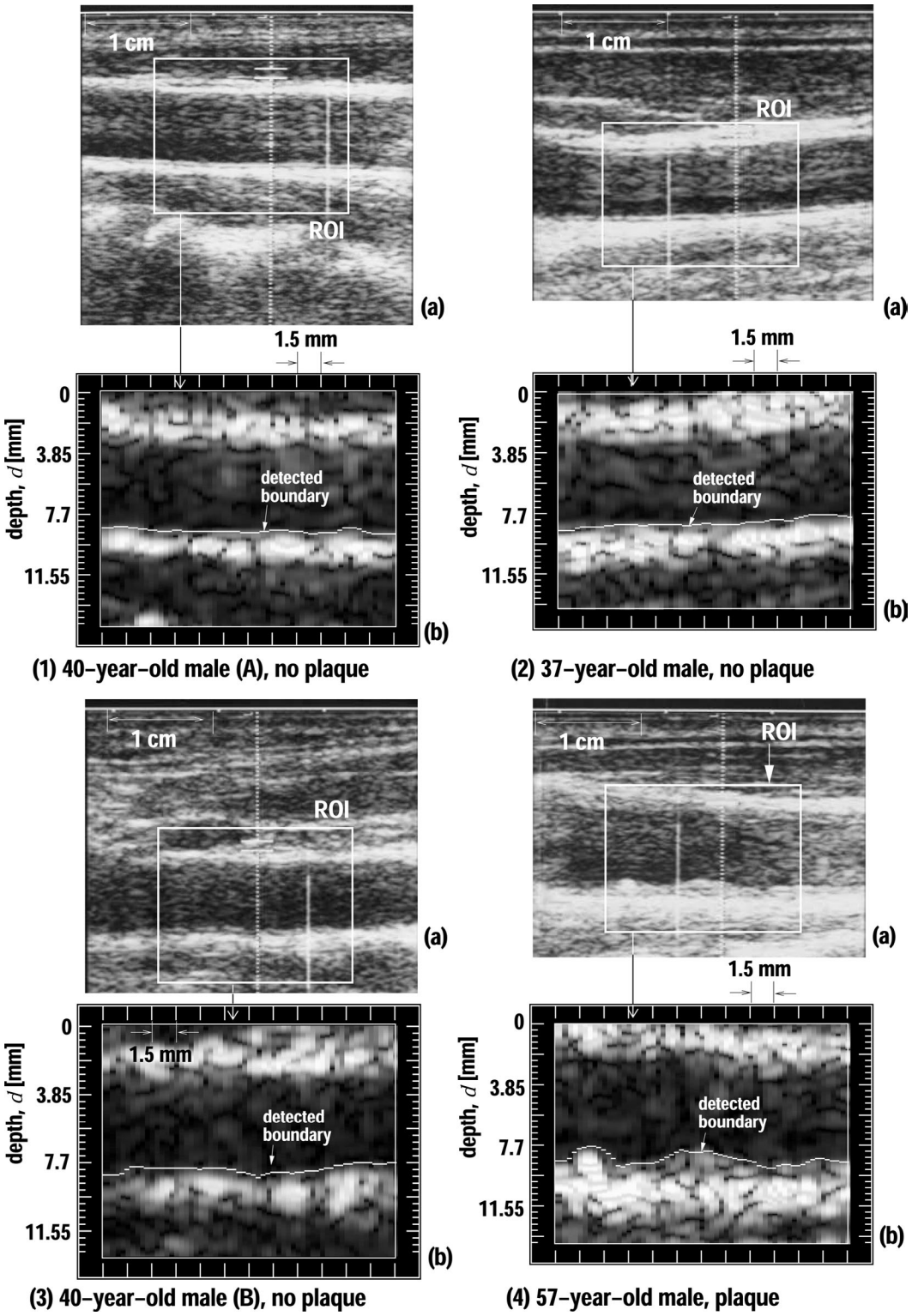

Fig. 12. Detected lumen-intima boundaries for four subjects. (a) B-mode image obtained by standard ultrasonic diagnostic equipment. (b) B-mode image reconstructed from the amplitude, $|z(t; d; \ell)|$, of the quadrature demodulated signal. (1) 40-year-old male (A) without atherosclerotic plaque. (2) 37-year-old male without atherosclerotic plaque. (3) 40-year-old male (B) without atherosclerotic plaque. (4) 57-year-old male with atherosclerotic plaque.

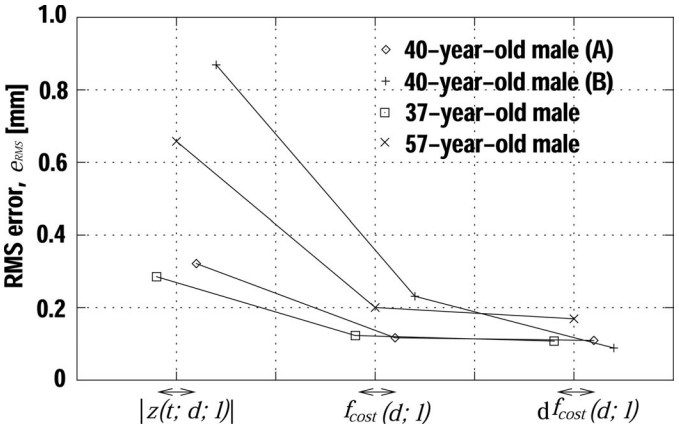

Fig. 13. RMS error, e_{RMS}, of the detected lumen-intima boundaries of each subject determined using the amplitude, $|z(t;d;\ell)|$, of the quadrature demodulated signal, cost function, $f_{\mathrm{cost}}(d;\ell)$, and spatial derivative, $\mathrm{d}f_{\mathrm{cost}}(d;\ell)$, of the cost function.

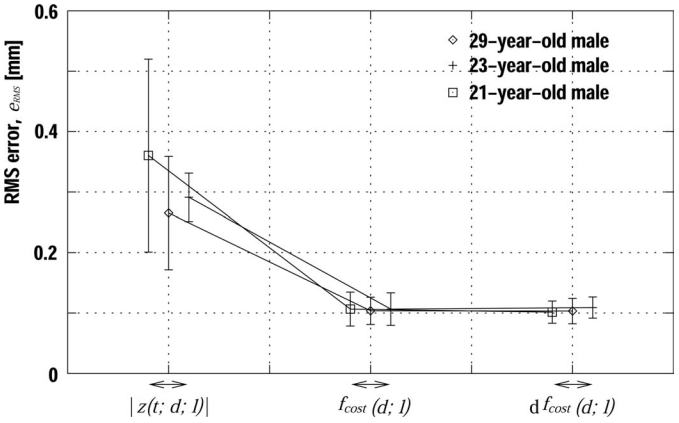

Fig. 14. Mean value and standard deviation of RMS error in the detected lumen-intima boundary of the posterior wall for five measurements. Mean values and standard deviations are evaluated for three subjects (29-year-old male, 23-year-old male, and 21-year-old male).

which was determined in Section III-D, was used. Fig. 14 shows mean values and standard deviations of RMS error of the detected lumen-intima boundary of the posterior wall for five measurements with respect to the three subjects. In Fig. 14, the RMS error of the detected boundary is improved using the proposed cost function in comparison with the amplitude-based detection. Furthermore, the lumen-intima boundary was detected with good reproducibility for five measurements using the proposed cost function.

C. Boundary Detection of the Anterior Wall

In this paper, a method for detection of the lumen-intima boundary of the posterior wall is proposed. However, to obtain the elastic modulus by (4), the luminal boundary of the anterior wall must be detected to obtain the inner radius, r_0, of the artery.

In the boundary detection of the anterior wall using $\mathrm{d}f_{\mathrm{cost}}(d;\ell)$, the threshold level must be higher than that in detection of the posterior wall because there are many signals in the lumen around the anterior wall due to the influence of the multiple reflection from the anterior wall and scattering from the tissue between the anterior wall and the skin surface. Fig. 15(a) shows the detected lumen-intima boundary of the anterior wall for the same data shown in Fig. 2(b) using the spatial derivative, $\mathrm{d}f_{\mathrm{cost}}(d;\ell)$, of the cost function. To improve the detection error, the detected boundary is laterally averaged within ± five ultrasonic beam positions. The threshold level is set at 0.0019 with the same procedure as described in Section III-D using 21 data sets. In Fig. 15(a), the detection error is large due to the signals in the lumen. Supposedly the luminal boundary of the anterior wall can be approximately detected from the maximum gradient of the peak in $\mathrm{d}f_{\mathrm{cost}}(d;\ell)$ in the vicinity of the anterior wall. For this purpose, the second order spatial derivative, $f''_{\mathrm{cost}}(d;\ell)$, of the cost function is obtained as shown in Fig. 15(c) by applying the same procedure as described in Section II-C to $\mathrm{d}f_{\mathrm{cost}}(d;\ell)$ as follows:

$$f''_{\mathrm{cost}}(d;\ell) = \frac{COV_2(d;\ell)}{VAR_2(d;\ell)}, \tag{28}$$

where

$$\begin{aligned} COV_2(d;\ell) =& \frac{1}{(M_{d2}+1)(N+1)} \sum_{m=-M_{d2}/2}^{M_{d2}/2} \sum_{n=-N/2}^{N/2} \\ & (d+mD)\cdot \mathrm{d}f_{\mathrm{cost}}(d+mD;\ell+nL) \\ & - \bar{d}\cdot\overline{\mathrm{d}f}_{\mathrm{cost}}, \end{aligned} \tag{29}$$

$$VAR_2(d;\ell) = \frac{1}{M_{d2}+1} \sum_{m=-M_{d2}/2}^{M_{d2}/2} (d+mD)^2 - \bar{d}^{\,2}, \tag{30}$$

$$\begin{aligned} \overline{\mathrm{d}f}_{\mathrm{cost}} =& \frac{1}{(M_{d2}+1)(N+1)} \sum_{m=-M_{d2}/2}^{M_{d2}/2} \sum_{n=-N/2}^{N/2} \\ & \mathrm{d}f_{\mathrm{cost}}(d+mD;\ell+nL), \end{aligned} \tag{31}$$

$$\bar{d} = \frac{1}{M_{d2}+1} \sum_{m=-M_{d2}/2}^{M_{d2}/2} (d+mD), \tag{32}$$

where M_{d2} is set at 4.

Fig. 15(b) shows the luminal boundary detected from the positive peak of $f''_{\mathrm{cost}}(d;\ell)$. As well as Fig. 15(b), the luminal boundaries of the anterior wall are detected for four other data shown in Fig. 12, and the RMS error of the detected boundary from the manually assigned boundary for each data set is evaluated as shown in Fig. 15(d). In Fig. 15(d), the RMS error is improved using $f''_{\mathrm{cost}}(d;\ell)$. However, the RMS error is rather large in comparison with the case of the posterior wall using $\mathrm{d}f_{\mathrm{cost}}(d;\ell)$. To improve the boundary detection of the anterior wall, further investigation is necessary to develop a method for further suppression of the signals in the lumen.

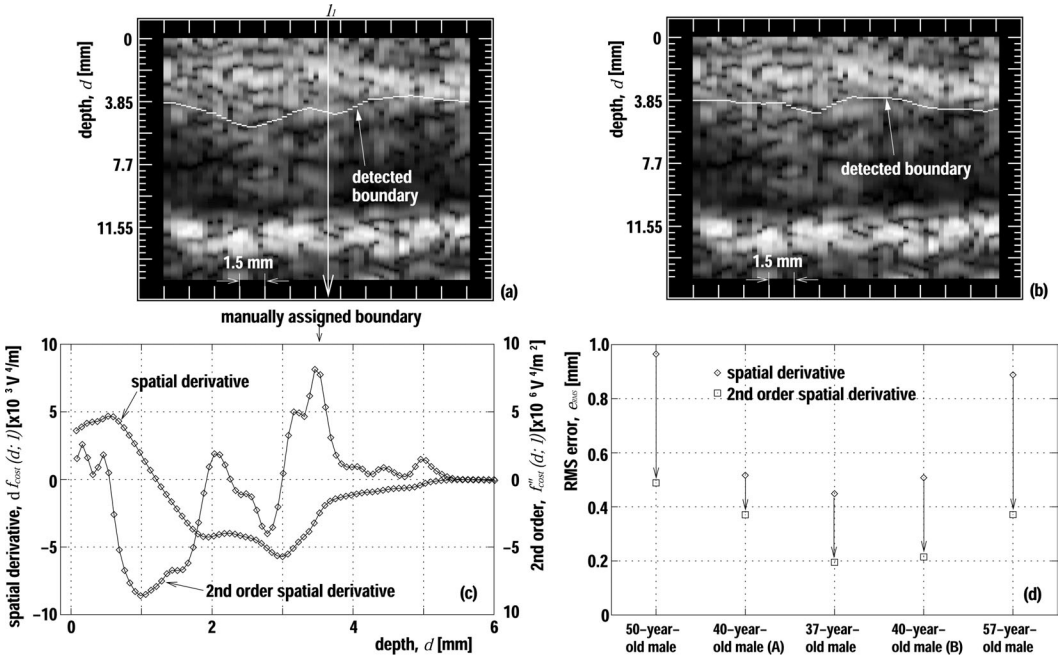

Fig. 15. Boundary detection of the anterior wall. (a) Detected boundary using the spatial derivative, $\mathrm{d}f_{\rm cost}(d;\ell)$, of the cost function. (b) Detected boundary using the second order spatial derivative, $f''_{\rm cost}(d;\ell)$. (c) $\mathrm{d}f_{\rm cost}(d;\ell_1)$ and $f''_{\rm cost}(d;\ell_1)$ plotted as a function of depth. (d) RMS errors, $e_{\rm RMS}$, of the detected boundaries for five subjects.

V. Conclusions

In this paper, we have proposed the use of the cost function for differentiation of the arterial wall from the lumen. From findings of in vivo experiments, it was shown that the lumen-intima boundary can be detected with an error of about 0.1 mm using the proposed cost function. This error is somewhat worse than that with other sophisticated methods based upon the amplitude of the echo. Using a single M-line signal, Hoeks *et al.* [40] detected the lumen-intima boundary with an error of 0.044 mm. Although their method achieves high accuracy using the temporally averaged envelope of the RF signal, the displacements at each depth along an ultrasonic beam must be estimated prior to temporal averaging of the envelope. Therefore, a large amount of computation is necessary to apply this method to the B-mode (many M-lines) images.

Although the accuracy of the proposed method is somewhat worse than that of such a sophisticated method, the proposed method requires only short analysis time (0.26 s, Pentium III 1.2 GHz) and thus is useful for the real-time measurement of the elasticity of the arterial wall. However, a method for detection of the outer boundary of the adventitia of the posterior wall and the luminal boundary of the anterior wall also must be established through further investigation to realize the real-time elasticity measurement by our method.

Acknowledgment

The authors would like to thank Dr. Jens E. Wilhjelm at the Technical University of Denmark for general discussions. The authors also acknowledge the comments made by the reviewers.

References

[1] R. T. Lee and P. Libby, "The unstable atheroma," *Arterioscler. Thromb. Vasc. Biol.*, vol. 17, pp. 1859–1867, 1997.

[2] S. Kiechl and J. Willeit, "The natural course of atherosclerosis. Part I: Incidence and progression," *Arterioscler. Thromb. Vasc. Biol.*, vol. 19, pp. 1484–1490, 1999.

[3] R. Smedby, "Do plaques grow upstream or downstream? An angiographic study in the femoral artery," *Arterioscler. Thromb. Vasc. Biol.*, vol. 17, pp. 912–918, 1997.

[4] F. A. Jaffer, C. J. O'Donnel, M. G. Larson, S. K. Chan, K. V. Kissinger, M. J. Kupka, C. Salton, R. M. Botnar, D. Levy, and W. J. Manning, "Age and sex distribution of subclinical aortic atherosclerosis: A magnetic resonance imaging examination of the framingham heart study," *Arterioscler. Thromb. Vasc. Biol.*, vol. 22, pp. 849–854, 2002.

[5] I. Wendelhag, O. Wiklund, and J. Wikstrand, "On quantifying plaque size and intima-media thickness in carotid and femoral arteries: Comments on results from a prospective ultrasound study in patients with familial hypercholesterolemia," *Arterioscler. Thromb. Vasc. Biol.*, vol. 16, pp. 843–850, 1996.

[6] S. Glagov, E. Weisenberg, C. K. Zarins, R. Stankunavicius, and G. J. Kolettis, "Compensatory enlargement of human atherosclerotic coronary arteries," *New Engl. J. Med.*, vol. 316, pp. 1371–1375, 1987.

[7] R. T. Lee, A. J. Grodzinsky, E. H. Frank, R. D. Kamm, and F. J. Schoen, "Structure-dependent dynamic mechanical behavior of fibrous caps from human atherosclerotic plaques," *Circulation*, vol. 83, pp. 1764–1770, 1991.

[8] H. M. Loree, A. J. Grodzinsky, S. Y. Park, L. J. Gibson, and R. T. Lee, "Static circumferential tangential modulus of human atherosclerotic tissue," *J. Biomech.*, vol. 27, pp. 195–204, 1994.

[9] P. C. G. Simons, A. Algra, M. L. Bots, D. E. Grobbee, and Y. van der Graaf, "Common carotid intima-media thickness and arterial stiffness," *Circulation*, vol. 100, pp. 951–957, 1999.

[10] E. Falk, P. K. Shah, and V. Fuster, "Coronary plaque disruption," *Circulation*, vol. 92, pp. 657–671, 1995.

[11] M. J. Davies, "Stability and instability: Two faces of coronary atherosclerosis," *Circulation*, vol. 94, pp. 2013–2020, 1996.

[12] J. Golledge, R. M. Greenhalgh, and A. H. Davies, "The symptomatic carotid plaque," *Stroke*, vol. 31, pp. 774–781, 2000.

[13] P. Hallock, "Arterial elasticity in man in relation to age as evaluated by the pulse wave velocity method," *Arch. Intern. Med.*, vol. 54, pp. 770–798, 1934.
[14] H. Kanai, M. Sato, Y. Koiwa, and N. Chubachi, "Transcutaneous measurement and spectrum analysis of heart wall vibrations," *IEEE Trans. Ultrason., Ferroelect., Freq. Contr.*, vol. 43, pp. 791–810, 1996.
[15] H. Kanai, H. Hasegawa, N. Chubachi, Y. Koiwa, and M. Tanaka, "Noninvasive evaluation of local myocardial thickening and its color-coded imaging," *IEEE Trans. Ultrason., Ferroelect., Freq. Contr.*, vol. 44, pp. 752–768, 1997.
[16] H. Kanai, K. Kawabe, M. Takano, R. Murata, N. Chubachi, and Y. Koiwa, "New method for evaluating local pulse wave velocity by measuring vibrations on aortic wall," *Electron. Lett.*, vol. 30, pp. 534–536, 1993.
[17] A. P. G. Hoeks, C. J. Ruissen, P. Hick, and R. S. Reneman, "Transcutaneous detection of relative changes in artery diameter," *Ultrasound Med. Biol.*, vol. 11, pp. 51–59, 1985.
[18] T. Länne, H. Stale, H. Bengtsson, D. Gustafsson, D. Bergqvist, B. Sonesson, H. Lecerof, and P. Dahl, "Noninvasive measurement of diameter changes in the distal abdominal aorta in man," *Ultrasound Med. Biol.*, vol. 18, pp. 451–457, 1992.
[19] A. P. G. Hoeks, X. Di, P. J. Brands, and R. S. Reneman, "Comparison of the performance of the RF cross correlation and Doppler autocorrelation technique to estimate the mean velocity of simulated ultrasound signals," *Ultrasound Med. Biol.*, vol. 19, pp. 727–740, 1993.
[20] P. J. Brands, A. P. Hoeks, M. C. Rutten, and R. S. Reneman, "A noninvasive method to estimate arterial impedance by means of assessment of local diameter change and the local center-line blood flow velocity using ultrasound," *Ultrasound Med. Biol.*, vol. 22, pp. 895–905, 1996.
[21] J. M. Meinders, P. J. Brands, J. M. Willigers, L. Kornet, and A. P. G. Hoeks, "Assessment of the spatial homogeneity of artery dimension parameters with high frame rate 2-D B-mode," *Ultrasound Med. Biol.*, vol. 27, pp. 785–794, 2001.
[22] D. H. Bergel, "The static elastic properties of the arterial wall," *J. Physiol.*, vol. 156, pp. 445–457, 1961.
[23] L. H. Peterson, R. E. Jensen, and J. Parnell, "Mechanical properties of arteries *in vivo*," *Circul. Res.*, vol. 8, pp. 622–639, 1960.
[24] K. Hayashi, H. Handa, S. Nagasawa, A. Okumura, and K. Moritake, "Stiffness and elastic behavior of human intracranial and extracranial arteries," *J. Biomech.*, vol. 13, pp. 175–184, 1980.
[25] O. Bonnefous, "Blood flow and tissue motion with ultrasound for vascular applications," *Comptes Rendus de l'Acadmie des Sci.–Series IV–Phys.*, vol. 2, no. 8, pp. 1161–1178, 2001.
[26] C. L. de Korte, E. I. Céspedes, A. F. W. van der Steen, and C. T. Lanée, "Intravascular elasticity imaging using ultrasound: Feasibility studies in phantoms," *Ultrasound Med. Biol.*, vol. 23, no. 5, pp. 735–746, 1997.
[27] E. I. Céspedes, C. L. de Korte, and A. F. W. van der Steen, "Intraluminal ultrasonic palpation: Assessment of local and cross-sectional tissue stiffness," *Ultrasound Med. Biol.*, vol. 26, no. 3, pp. 385–396, 2000.
[28] H. Hasegawa, H. Kanai, N. Hoshimiya, N. Chubachi, and Y. Koiwa, "Accuracy evaluation in the measurement of a small change in the thickness of arterial walls and the measurement of elasticity of the human carotid artery," *Jpn. J. Appl. Phys.*, vol. 37, pp. 3101–3105, 1998.
[29] H. Hasegawa, H. Kanai, N. Hoshimiya, and Y. Koiwa, "Reduction of influence of decrease in signal-to-noise ratio in measurement of change in thickness of arterial wall due to heartbeat," *Jpn. J. Appl. Phys.*, vol. 39, pp. 3257–3261, 2000.
[30] H. Hasegawa, H. Kanai, and Y. Koiwa, "Modified phased tracking method for measurement of change in thickness of arterial wall," *Jpn. J. Appl. Phys.*, vol. 41, pp. 3563–3571, 2002.
[31] H. Hasegawa, H. Kanai, N. Chubachi, and Y. Koiwa, "Noninvasive evaluation of Poisson's ratio of arterial wall using ultrasound," *Electron. Lett.*, vol. 33, pp. 340–342, 1997.
[32] H. Kanai, H. Hasegawa, M. Ichiki, F. Tezuka, and Y. Koiwa, "Elasticity imaging of atheroma with transcutaneous ultrasound. Preliminary study," *Circulation*, vol. 107, pp. 3018–3021, 2003.
[33] M. L. Hijmering, E. S. G. Stroes, G. Pasterkamp, M. Sierevogel, J. D. Banga, and T. J. Rabelink, "Variability of flow mediated dilation: Consequences for clinical application," *Atherosclerosis*, vol. 157, pp. 369–373, 2001.
[34] L. Fan, P. Santago, W. Riley, and D. M. Herrington, "An adaptive template-matching method and its application to the boundary detection of brachial artery ultrasound scans," *Ultrasound Med. Biol.*, vol. 27, pp. 399–408, 2001.
[35] R. W. Stadler, W. C. Karl, and R. S. Lees, "New methods for arterial diameter measurement from B-mode images," *Ultrasound Med. Biol.*, vol. 22, pp. 25–34, 1996.
[36] F. Beux, S. Carmassi, M. V. Salvetti, L. Ghiadoni, Y. Huang, S. Taddei, and A. Salvetti, "Automatic evaluation of arterial diameter variation from vascular echographic images," *Ultrasound Med. Biol.*, vol. 27, pp. 1621–1629, 2001.
[37] V. R. Newey and D. K. Nassiri, "Online artery diameter measurement in ultrasound images using artificial neural networks," *Ultrasound Med. Biol.*, vol. 28, pp. 209–216, 2002.
[38] Q. Liang, I. Wendelhag, J. Wilstrand, and T. Gustavsson, "A multiscale dynamic programming procedure for boundary detection in ultrasonic artery images," *IEEE Trans. Med. Imag.*, vol. 19, pp. 127–142, 2000.
[39] J. D. Klingensmith, R. Shekhar, and D. G. Vince, "Evaluation of three-dimensional segmentation algorithms for the identification of luminal and media-adventitial borders in intravascular ultrasound images," *IEEE Trans. Med. Imag.*, vol. 19, pp. 996–1011, 2000.
[40] A. P. G. Hoeks, C. Willekes, P. Boutouyrie, P. J. Brands, J. M. Willigers, and R. S. Reneman, "Automated detection of local artery wall thickness based on M-line signal processing," *Ultrasound Med. Biol.*, vol. 23, pp. 1017–1023, 1997.
[41] C. Willekes, A. P. G. Hoeks, M. L. Bots, P. J. Brands, J. M. Willigers, and R. S. Reneman, "Evaluation of off-line automated intima-media thickness detection of the common carotid artery based on M-line signal processing," *Ultrasound Med. Biol.*, vol. 25, pp. 57–64, 1999.

Hideyuki Hasegawa was born in Oyama, Japan, in 1973. He received the B.E. degree in electrical engineering from Tohoku University, Sendai, Japan, in 1996. He received the Ph.D. degree in electrical engineering from Tohoku University in 2001. He is presently a research associate of Graduate School of Engineering of Tohoku University. His main research interest is medical ultrasound, especially diagnosis of atherosclerosis based on measurement of mechanical properties of arterial wall.

Dr. Hasegawa is a member of the IEEE, the Acoustical Society of Japan, the Japan Society of Ultrasonics in Medicine, and the Institute of Electronics, Information and Communication Engineers.

Hiroshi Kanai (A'88–M'91) was born in Matsumoto, Japan, on November 29, 1958. He received the B.E. degree in electrical engineering from Tohoku University, Sendai, Japan in 1981, and the M.E. and Ph.D. degrees, also from Tohoku University, in 1983 and in 1986, both in electrical engineering.

From 1986 to 1988 Dr. Kanai was with the Education Center for Information Processing, Tohoku University, as a research associate. From 1990 to 1992 he was a lecturer in the Department of Electrical Engineering, Faculty of Engineering, Tohoku University. From 1992 to 2001 he was an associate professor in the Department of Electrical Engineering, Faculty of Engineering, Tohoku University. Since 2001 he has been a professor in the Department of Electronic Engineering, Graduate School of Engineering, Tohoku University.

His present interests are in ultrasonic measurement and digital signal processing for diagnosis of heart diseases and arteriosclerosis.

Dr. Kanai is a member of the IEEE, the Acoustical Society of Japan, the Institute of Electronics Information and Communication Engineering of Japan, the Japan Society of Mechanical Engineers, the

Japan Society of Ultrasonics in Medicine, Japan Society of Medical Electronics and Biological Engineering, and the Japanese Circulation Society.

Yoshiro Koiwa was born in Sendai, Japan, in 1944. He graduated from Tohoku University, Sendai, Japan, in 1969. He received the M.D. degree from Tohoku University in 1977.

He is presently an associate professor of internal medicine of Tohoku University. His main research interest is cardiovascular disease, especially cardiac function and heart failure.

Dr. Koiwa is a member of the Japanese Circulation Society, and the Japan Society of Medical Electronics and Biological Engineering.